Size and load effects on the biaxial fatigue resistance of holed structural components

A. Carpinteri, L. Montanari, A. Spagnoli, S. Vantadori
Department of Civil-Environmental Engineering, University of Parma, Parma (Italy)
spagnoli@unipr.it

ABSTRACT. A high-cycle multiaxial fatigue criterion, based on a combined critical point method-critical plane approach, is used to estimate the multiaxial endurance limit in notched metal structural components. Accordingly, the position of the critical point and the orientation of the critical plane (plane where fatigue strength assessment has to be performed) are determined on the basis of some pseudo-isostatic lines related to the stress fields experiencing, at each material point, the maximum principal stress in the loading cycle. Some experimental results related to holed steel specimens subjected to in-phase and out-of-phase axial and torsional loading are analysed. The comparison between experimental results and theoretical values determined through the above criterion is instrumental in highlighting the notch size-effect (as the hole diameter varies) under uniaxial and biaxial far-field stress conditions as well as the effect of the loading phase.

SOMMARIO. Un criterio di resistenza a fatica multiassiale ad alto numero di ciclo, formulato combinando il metodo del punto critico con l'approccio del piano critico, è utilizzato per predire la resistenza a fatica multiassiale in componenti strutturali metallici intagliati. La posizione del punto critico e l'orientazione del piano critico (piano su cui viene effettuata la verifica di resistenza a fatica) sono determinati sulla base di una sorta di linee isostatiche relative a campi tensionali corrispondenti, in ciascun punto materiale, alla massima tensione principale di trazione durante un ciclo di carico. Vengono analizzati alcuni risultati sperimentali relativi a provini d'acciaio contenenti piccoli fori, soggetti a carichi assiali e torsionali in fase e fuori fase. Il confronto tra tali risultati sperimentali e i valori ottenuti mediante il suddetto criterio evidenzia sia l'effetto della dimensione dell'intaglio sulla resistenza a fatica in condizioni di sforzo remoto mono e biassiale sia l'effetto della non proporzionalità del carico.

KEYWORDS. Critical plane approach; Fatigue strength; Multiaxial fatigue; Notch fatigue.

INTRODUCTION

Fatigue failures in structural components almost invariably occur at stress concentrators such as notches and material flaws. Circular holes are the geometrically simplest stress concentrators. Nevertheless, when submitted to multiaxial remote cyclic loading, they produce a variety of different stress field features (in their vicinity) which influence the fatigue resistance of the structural components [1-5].
The high-cycle uniaxial fatigue resistance of notched components can be assessed by means of critical distance approaches [6-10]. Accordingly, the fatigue assessment is performed by considering the relevant stress component in a critical point at a certain distance from the notch root or by averaging a relevant stress component over a linear path emanating from

the notch root or over a volume ahead of the notch. When a notched structural component is subjected to multiaxial cyclic loading, appropriate stress components must be selected in order to exploit the above critical-distance approaches, and a multiaxial fatigue criterion must be applied (e.g. see [11]).
Some years ago, the present authors proposed a high-cycle critical plane-based multiaxial fatigue criterion [12] suitable for smooth components. Such a criterion has recently been extended to notched components under multiaxial loading by employing a critical point method [13,14]. In the present paper, a simplified version of this criterion [15,16] is applied in combination with a critical point approach. For the case of holed structural components under biaxial non-proportional remote loading, the choice of the appropriate path for determining the position of the critical point is discussed. In the presentation of the results, emphasis is placed on the effects of hole size, biaxiality ratio and load phase on the multiaxial fatigue resistance.

DEFINITION OF THE EQUIVALENT STRESS ACTING ON THE CRITICAL PLANE

A multiaxial fatigue criterion based on the so-called critical plane approach has been proposed by Carpinteri and Spagnoli (C-S criterion) [12-14] to estimate the high-cycle fatigue strength (either endurance limit or fatigue lifetime) of both smooth and notched metallic structural components submitted to any periodic proportional or non-proportional multiaxial loading. Then, a simplified version of the C-S criterion has been presented in Refs [15, 16]. The main steps of the simplified C-S criterion are as follows:

- ✓ Averaged directions of the principal stress axes are determined on the basis of their instantaneous directions;
- ✓ The orientation of the critical plane (also termed verification plane) is linked to the averaged directions of the principal stress axes. Two material parameters are required at this step: fatigue strength $\sigma_{af,-1}$ (under fully reversed normal stress) and fatigue strength $\tau_{af,-1}$ (under fully reversed shear stress) at a reference number of loading cycles;
- ✓ The mean value and the amplitude (in a loading cycle) of the normal stress and shear stress, respectively, acting on the critical plane are computed;
- ✓ The fatigue strength estimation is performed via a quadratic combination of normal and shear stress components acting on the critical plane. In the case of finite-life fatigue evaluation, two further material parameters are required at this step, namely the slopes of the *S-N* curve in the high-cycle regime under fully reversed normal stress and fully reversed shear stress, respectively.

At a given material point P, the direction cosines of the instantaneous principal stress directions 1, 2 and 3 (being $\sigma_1(t) \geq \sigma_2(t) \geq \sigma_3(t)$) with respect to a fixed $PXYZ$ frame can be worked out from the time-varying stress tensor $\boldsymbol{\sigma}(t)$. Then the orthogonal coordinate system $P123$ with origin at point P and axes coincident with the principal stress directions can be defined through the principal Euler angles, ϕ, θ, ψ, whose ranges at the end of a two-stage reduction procedure [12] are as follows: $0 \leq \phi,\ \theta \leq \pi/2$ and $-\pi/2 < \psi \leq \pi/2$.

The averaged directions of the principal stress axes $\hat{1}, \hat{2}, \hat{3}$ are obtained from the averaged values $\hat{\phi}, \hat{\theta}, \hat{\psi}$ of the principal Euler angles. Such values are computed by independently averaging the instantaneous values $\phi(t), \theta(t), \psi(t)$, as follows [16]:

$$\hat{\phi} = \int_0^T \phi(t) W(t) dt \qquad \hat{\theta} = \int_0^T \theta(t) W(t) dt \qquad \hat{\psi} = \int_0^T \psi(t) W(t) dt \tag{1}$$

with T = period of the loading cycle. By assuming the following weight function $W(t)$:

$$W(t) = H\left[\sigma_1(t) - \sigma_{1,\max}\right] \quad \text{with} \quad \begin{matrix} H[x] = 1 \ \ for \ \ x \geq 0 \\ H[x] = 0 \ \ for \ \ x < 0 \end{matrix} \tag{2}$$

where $\sigma_{1,\max}$ is the maximum value (in the loading cycle) of the maximum (tensile) principal stress σ_1. Note that, according to the weight function in Eq. 2, no averaging procedure is actually required since the averaged principal stress

axes coincide with the instantaneous principal directions corresponding to the time instant at which the maximum principal stress σ_1 achieves its maximum value during the loading cycle, and this makes the implementation of the criterion straightforward.

The orientation of the critical plane is correlated with the averaged directions of the principal stress axes [12]. In more detail, the empirical expression for δ (δ = angle between the normal w to the critical plane and the averaged direction $\hat{1}$ of the maximum principal stress, where w belongs to the principal plane $\hat{1}\hat{3}$) is assumed to be as follows:

$$\delta = \frac{3\pi}{8}\left[1 - \left(\frac{\tau_{af,-1}}{\sigma_{af,-1}}\right)^2\right] \tag{3}$$

Equation 3 is valid for hard metals which are characterised by values of the ratio $\tau_{af,-1}/\sigma_{af,-1}$ ranging from $1/\sqrt{3}$ to 1 (note that the lower limit of $\tau_{af,-1}/\sigma_{af,-1}$ corresponds to the Von Mises strength criterion of mild metals for static loading). In the light of the above, the orientation of the critical plane depends on the time-varying stress state as well as the material parameters $\sigma_{af,-1}$ and $\tau_{af,-1}$.

For multiaxial constant-amplitude cyclic loading, the normal stress vector N and the shear stress vector C lying on the critical plane are periodic functions of time. The direction of the normal stress $N(t)$ is fixed with respect to time: consequently, the mean value N_m and the amplitude N_a of the normal stress can readily be calculated. On the other hand, the definitions of the shear stress mean value C_m and amplitude C_a are not unique, due to the generally time-varying direction of C. The procedure proposed by Papadopoulos [17] is applied to determine C_m and C_a [12-16].

As is well-known, the effect of a tensile mean normal stress superimposed upon an alternating normal stress strongly reduces the fatigue resistance of metals, while a mean shear stress superimposed upon an alternating shear stress does not affect the fatigue life. Therefore, the following multiaxial fatigue strength condition is adopted [16]:

$$\left(\frac{N_{a,eq}}{\sigma_{af,-1}}\right)^2 + \left(\frac{C_a}{\tau_{af,-1}}\right)^2 = 1 \tag{4}$$

where the equivalent normal stress amplitude acting on the critical plane is given by:

$$N_{a,eq} = N_a + \sigma_{af,-1}\left(\frac{N_m}{\sigma_u}\right) \tag{5}$$

with σ_u = ultimate tensile strength. Eq. 5 is based on the well-known linear interaction between normal stress amplitude and normal stress mean value (diagram of Goodman).

Finally, in order to transform the actual periodic multiaxial stress state into an equivalent uniaxial normal stress state (with amplitude $\sigma_{a,eq}$), Eq. 4 can be rewritten as follows:

$$\sigma_{a,eq} = \sqrt{N_{a,eq}^2 + \left(\frac{\sigma_{af,-1}}{\tau_{af,-1}}\right)^2 C_a^2} = \sigma_{af,-1} \tag{6}$$

POSITION OF THE CRITICAL POINT

Consider a traction-free notch surface contained in a body submitted to a constant-amplitude loading. At any point on the notch surface, a principal stress is always null and its direction is normal to the notch surface. The point H of crack initiation (the so-called hot spot) on the notch surface (see Fig. 1 where, for the sake of simplicity, a plane

stress/strain situation is considered) is assumed as that point experiencing the maximum value of $\sigma_{a,eq}$ (Eq. 6). Note that, under any applied multiaxial loading, principal stress directions on the notch surface are fixed with respect to time and, hence, averaged principal stress directions $\hat{1}$ and $\hat{3}$ are those depicted in Fig. 1 ($\hat{1}$ is tangent to the notch surface and $\hat{3}$ is normal to such a surface). Consequently, the hot spot corresponds to the point (on the notch surface) where the amplitude of the maximum principal stress attains the greatest value.
Along the mainstream of the critical distance theory proposed by Taylor [10], we consider hereafter a critical point approach. Accordingly, the endurance limit condition in a notched structural component occurs when the amplitude of a selected stress component, computed through a linear elastic analysis at a certain distance from the notch tip, is equal to $\sigma_{af,-1}$. Such a distance is equal to $L/2$, where L is the ElHaddad intrinsic crack length [18], that is:

$$L = \frac{1}{\pi}\left(\frac{\Delta K_{I,th}}{2\sigma_{af}}\right)^2 \tag{7}$$

$\Delta K_{I,th}$ being the threshold range of the stress intensity factor for long cracks. Note that the two material parameters in Eq. 7 should be related to the same loading ratio.
In the following, we consider two alternatives to define the path along which the position of the critical point P is calculated: (i) the critical point P is at a distance $L/2$ from the point H, measured along the direction normal to the notch surface; (ii) the critical point P is at a distance $L/2$ from the point H, measured along a generally curved path normal to the corresponding averaged direction $\hat{1}$ of the maximum principal stress, described in the previous section. In other words, the path of the definition (ii) corresponds to pseudo-isostatic compressive lines related to the stress fields experiencing, at each material point, the maximum principal stress in the loading cycle. Note that the definition (i) is slightly different from that proposed in Refs [13, 14].
Once the position of the critical point P is determined according to the above two definitions, the stress tensor at such a point is processed through the C-S criterion described in the previous section.

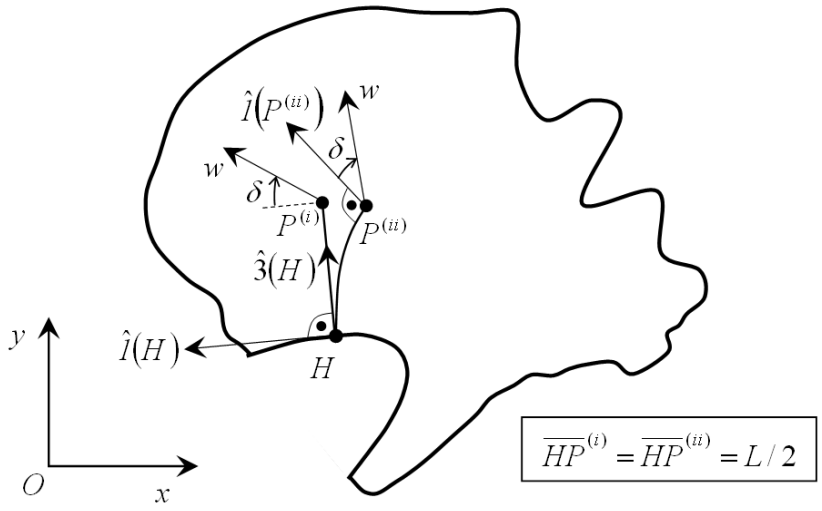

Figure 1: Position of the hot spot H and two alternative definitions of the path for calculating the position of the critical point P in the case of a general traction-free notch surface (plane stress/strain conditions are assumed).

COMPARISON WITH EXPERIMENTAL RESULTS

Some experimental results concerning round bars with artificially drilled surface holes under proportional and non-proportional loadings are considered [19, 20]. The specimens, having a hole with diameter D ranging from 40 to 500 μm, are subjected to fully reversed bending or torsion or combined in-phase and $\pi/2$ out-of-phase bending

and torsion. Two materials are analysed: 0.37%*C* annealed carbon steel (JIS S35C) with Vickers hardness equal to 160, $\sigma_{af,-1}$ = 233 MPa, $\tau_{af,-1}$ = 145 MPa; chrome-molybdenum quenched and tempered steel (JIS SCM435) with Vickers hardness equal to 327, $\sigma_{af,-1}$ = 379 MPa, $\tau_{af,-1}$ = 218 MPa.

Due to the lack of experimental data, the ElHaddad distance *L* is determined, as is suggested for instance in Ref. [21], by knowing the experimental fatigue limit under uniaxial loading of a smooth specimen and a single holed specimen. Accordingly, the distance *L*/2 from the notch surface is that at which the equivalent stress $\sigma_{a,eq}$, calculated according to Eq. 6 for the stress level corresponding to the fatigue limit of the holed specimen, is equal to the fatigue strength for smooth specimens $\sigma_{af,-1}$. The calculated distance L/2 from the notch surface is equal to 37.6μm for JIS S35C steel and 38.2μm for JIS SCM435 steel.

The applied far-field stress amplitudes $\sigma_{x,a}$ (due to bending) and $\tau_{xy,a}$ (due to torsion) are shown in Fig. 2, where the *xy* plane is tangent to the bar surface in the hole centre. The stress state in the vicinity of the hole is here determined according to the Kirsch solution for plane stress state [22]. The values of the biaxiality ratio $\lambda = \tau_{xy,a}/\sigma_{x,a}$ considered in the experimental tests are: 0 (pure bending), 0.5, 1.0, 2.0, ∞ (pure torsion). The phase angle γ between the two applied stress components is equal to 0 (proportional loading) and $\pi/2$ (non-proportional loading).

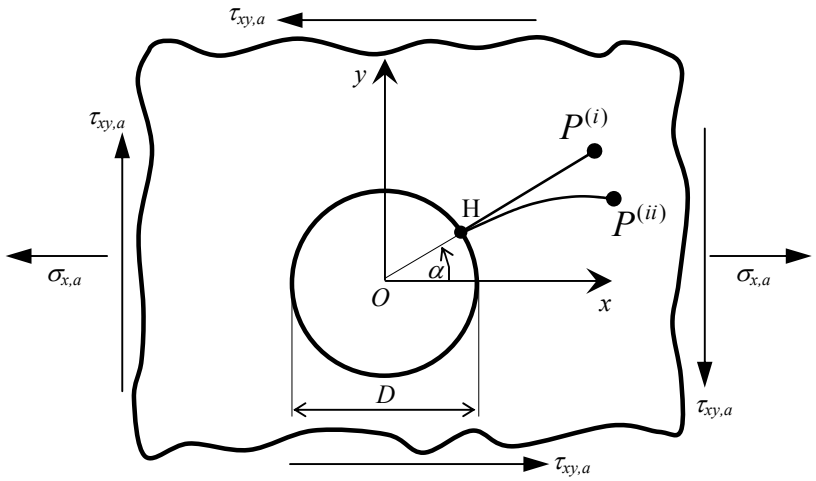

Figure 2: Normal and shear stresses acting on a specimen with a circular hole of diameter *D*. The position of the hot-spot is defined by the angle α.

As far as the position of the hot spot H is concerned (Fig. 2), it has been demonstrated analytically [14] that, for phase angle γ equal to 0, $\alpha = \pi/2 - \alpha'$ with $k = 1,3$ and $\alpha' = \frac{1}{2}\arctan 2\lambda$ ($\alpha' \in [0,\pi/4]$). On the other hand, for $\gamma = \pi/2$, we have $\alpha = k\pi \pm \alpha''$ for $\lambda > \sqrt{3/8}$ with $k = 0,1$ and $\alpha'' = \frac{1}{2}\arccos\left(2 - 8\lambda^2\right)^{-1}$ ($\alpha'' \in [\pi/4,\pi/2]$), and $\alpha = \pm\pi/2$ for $\lambda \le \sqrt{3/8}$. Hence, the hot spot position exhibits a multiplicity 4 when $\gamma = \pi/2$ and $\lambda > \sqrt{3/8}$, and a multiplicity 2 in the remaining cases. In Fig. 3, the hot spot position (see angle α in Fig.2, with $45° \le \alpha \le 90°$) as a function of the biaxiality ratio is reported for phase angle γ equal to 0 or $\pi/2$.

Fig. 4 illustrates the paths according to the definitions (i) and (ii) to calculate the position of the critical point P as the the biaxiality ratio λ and the phase angle γ are made to vary. Note that, in the case of holed specimens under pure bending ($\lambda = 0$) or under pure torsion ($\lambda = \infty$), the two definitions (i) and (ii) of the path along which the critical point P is located yield radial paths which are normal to the *x* axis (loading axis) and $\pi/4$-inclined with respect to the *x* axis, respectively.

The comparisons between experimental results [19, 20] and theoretical evaluations of fatigue limit as a function of the hole diameter for bending, torsion and combined bending and torsion are reported in Figs 5 and 6 for the two materials examined, respectively.

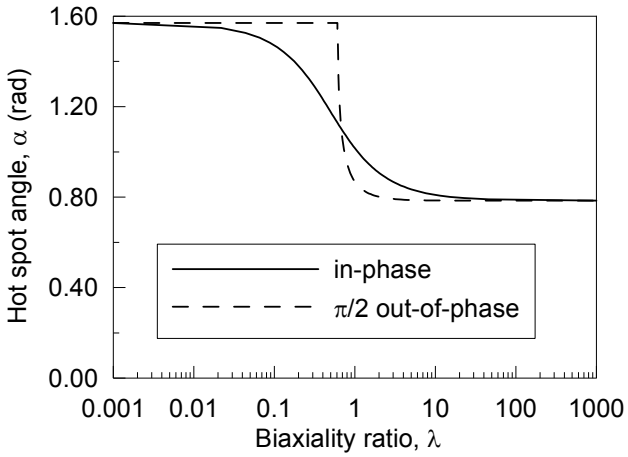

Figure 3: Hot spot position ($\alpha \in [\pi/4, \pi/2]$) as a function of biaxiality ratio λ and phase angle γ.

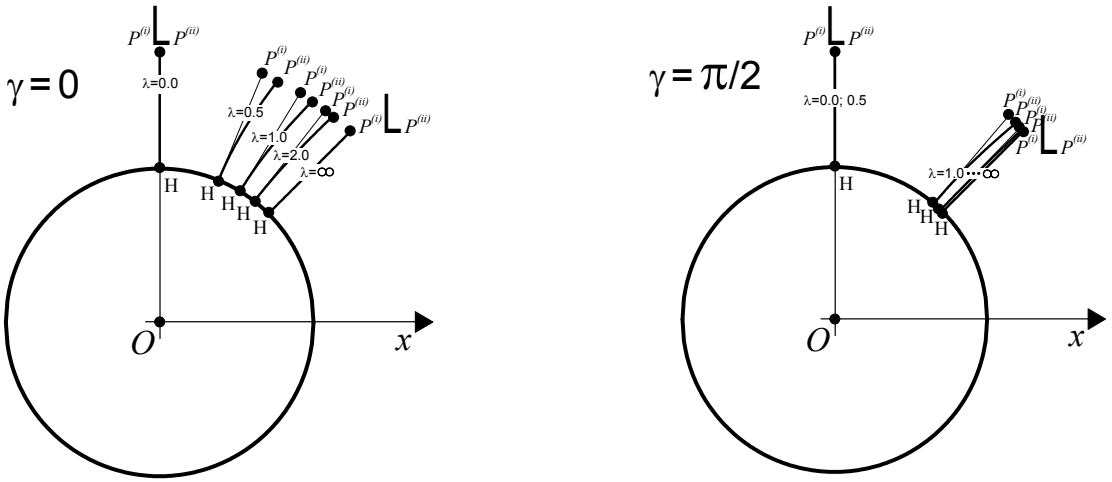

Figure 4: Paths emanating from the circular hole, for critical point calculation as the biaxiality ratio λ and the phase angle γ vary: (i) normal path; (ii) pseudo-isostatic path.

CONCLUSIONS

The present study represents an attempt to evaluate fatigue limit conditions for multiaxially-loaded notched structural components, by combining a critical plane-based criterion proposed by the authors with a critical-distance method. In particular, following the philosophy of the point method, fatigue limit conditions occur in a notched structural component subjected to far-field multiaxial loading when the amplitude of the equivalent normal stress, defined according to the proposed criterion, attains the normal stress fatigue limit for plain structural components in a point at a certain distance from the hot spot on the notch surface. Such a distance, which has to be regarded as a material constant, is chosen to be measured along two alternative paths (so-called normal path and pseudo-isostatic path). The comparison with some experimental results concerning circular notches shows a reasonably good evaluation capability of the proposed criterion. No significant differences are observed by changing the path for the critical point calculation. The theoretical results appear to correctly evaluate the notch size-effect as well as the effect of the loading phase observed in the experimental data.

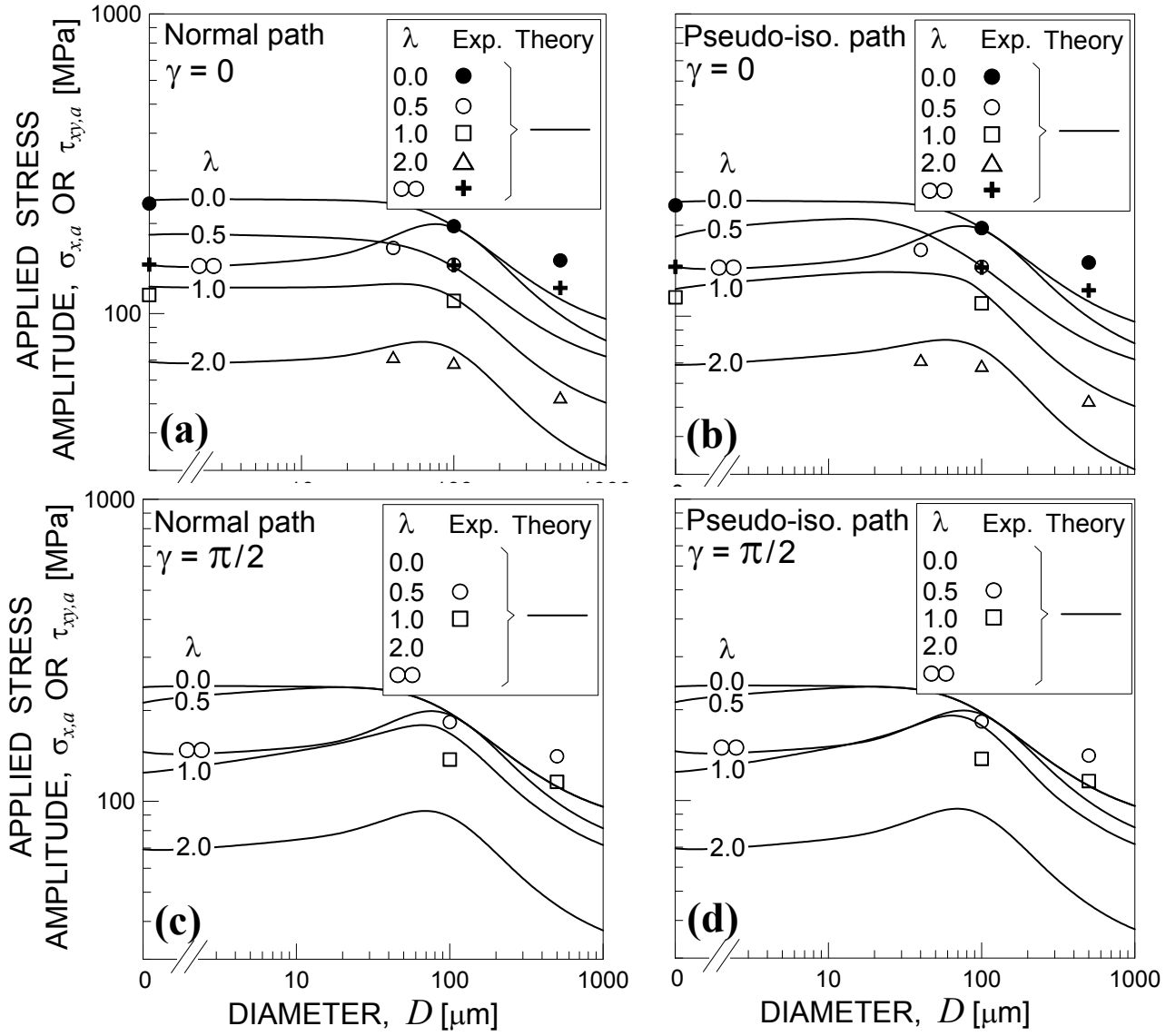

Figure 5: Experimental results [19, 20] and theoretical evaluations of fatigue limit as a function of the hole diameter for bending, torsion and combined bending and torsion (material JIS S35C).

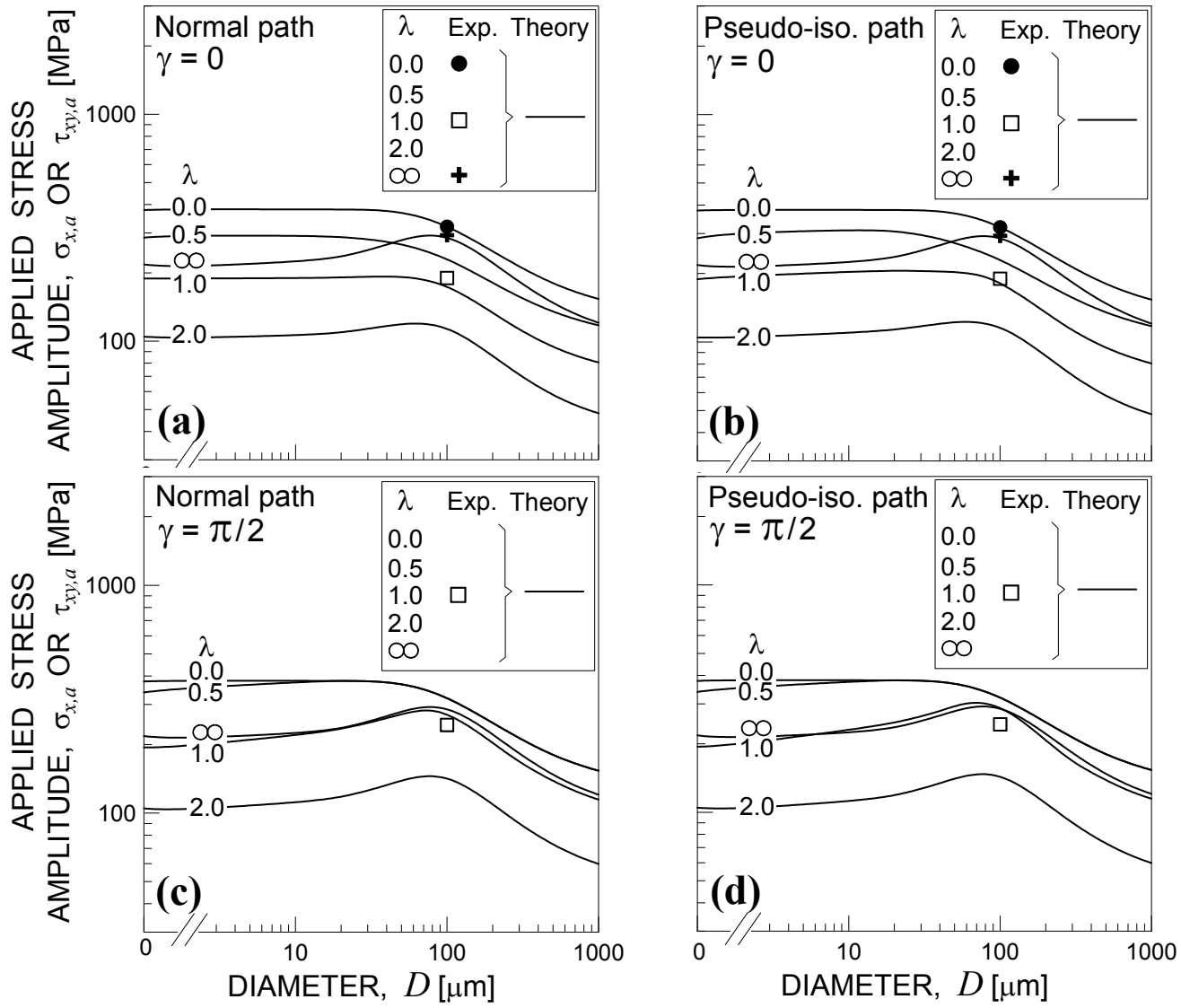

Figure 6: Experimental results [19, 20] and theoretical evaluations of fatigue limit as a function of the hole diameter for bending, torsion and combined bending and torsion (material JIS SCM435).

REFERENCES

[1] M. Endo, Y. Murakami, J. Engng. Mater. Technol. (ASME Trans.), 109 (1987) 124.
[2] S. Beretta, Y. Murakami, Fatigue Fract. Engng. Mater. Struct., 23 (2000) 97.
[3] M. Endo, In: Biaxial/Multiaxial Fatigue and Fracture, edited by An. Carpinteri, M. de Freitas, A. Spagnoli. ESIS Publication, Elsevier, 31 (2003) 243.
[4] A.J. McEvily, M. Endo, Int. J. Fatigue, 28 (2006) 504.
[5] K. Tanaka, K. Morita, Y. Akiniwa, Fatigue Fract. Engng. Mater. Struct., 31 (2008) 1079.
[6] R.E. Peterson. In: Metal Fatigue, edited by G. Sines, J.L. Waisman. McGraw-Hill (1959) 293.
[7] T. Isibasi, Fatigue of Metals and Prevention of Fracture, Yokendo, Tokyo (1967).
[8] K. Tanaka, Int. J. Fract., 22 (1983) R39.
[9] A. Seweryn, Z. Mroz, Int. J. Solids Struct., 35 (1998) 1589.
[10] D. Taylor, Int. J. Fatigue, 21 (1999) 413.
[11] L. Susmel, D. Taylor, Fatigue Fract. Engng. Mater. Struct., 26 (2003) 821.

[12] A. Carpinteri, A. Spagnoli, Int. J. Fatigue, 23 (2001) 135.
[13] A. Carpinteri, A. Spagnoli, S. Vantadori, D. Viappiani, Engng. Fract. Mechs., 75 (2008) 1864.
[14] A. Carpinteri, A. Spagnoli, S. Vantadori, D. Viappiani. In: 8th Int. Conference on Multiaxial Fatigue & Fracture (ICMFF8), on CD-Rom, Sheffield, UK (2007).
[15] A. Carpinteri, A. Spagnoli, S. Vantadori, Int. J. Fatigue, 31 (2009) 188.
[16] A. Carpinteri, A. Spagnoli, S. Vantadori, Int. J. Fatigue, 33 (2011) 969.
[17] I.V. Papadopoulos, Fatigue Fract. Engng Mater. Struct., 21 (1998) 269.
[18] M.H. ElHaddad, N.F. Dowling, T.H. Topper, K.N. Smith, Int. J. Fract., 16 (1980) 15.
[19] M. Endo, In: Small fatigue cracks: mechanics. Mechanisms and applications, edited by K.S. Ravichandran, R.O. Ritchie, Y. Murakami, (1999) 375.
[20] M. Endo, I. Ishimoto, Int. J. Fatigue, 28 (2006) 592.
[21] L. Susmel, D. Taylor, Fatigue Fract. Engng. Mater. Struct., 31 (2008) 1047.
[22] G. Kirsch, V.D.I., 42 (1898) 797-807.